Trapping and flow among random arrays of oriented spheroidal inclusions

C. A. Miller and I. C. Kim
Department of Mechanical and Aerospace Engineering, North Carolina State University, Raleigh, North Carolina 27695-7910

S. Torquato
Departments of Mechanical and Aerospace Engineering and of Chemical Engineering, North Carolina State University, Raleigh, North Carolina 27607-7910

(Received 6 November 1990; accepted 7 January 1991)

The effective trapping rate k associated with diffusion-controlled reactions among random distributions of spatially *correlated* and *uncorrelated*, oriented spheroidal traps of aspect ratio ϵ is determined from Brownian motion simulations. Data for k are obtained for prolate cases ($\epsilon = 2$, 5, and 10), oblate cases ($\epsilon = 0.1$, 0.2, and 0.5), and spheres ($\epsilon = 1$) over a wide range of trap volume fractions (ϕ_2) and satisfy recently obtained rigorous lower bounds on k for this statistically anisotropic model. The results for the trapping rate for correlated traps always bounds from above corresponding results for uncorrelated traps. Generally, the trapping rate k, for fixed ϕ_2, increases with decreasing aspect ratio ϵ, showing a precipitous rise in k as the spheroids become disklike. Using a recent theorem due to Torquato [Phys. Rev. Lett. **64**, 2644 (1990)], data for the trapping rate k can be employed to infer information about the fluid permeability tensor $\mathbf{K}$ associated with slow viscous flow through porous media composed of the same arrays of oriented spheroidal particles.

I. INTRODUCTION

Diffusion-controlled reactions arise in a host of phenomena, including heterogeneous catalysis, migration of atoms and defects in solids, combustion of liquid droplets, polymer chain growth kinetics, colloid or crystal growth, precipitation, and fluorescence quenching. A diffusion-controlled reaction is one in which the time for two bodies to diffuse in the same neighborhood is the rate-limiting step, the reaction time being negligible in comparison. Often one of the reaction partners is large and may be regarded as static. In such situations, therefore, one considers media composed of static traps (sinks) distributed throughout a region containing reactive particles. The reactant diffuses in the trap-free region but is instantly absorbed on contact with any trap. At steady state, the rate of production of the diffusing species is exactly compensated by its removal by the traps. At sufficiently low trap densities, such that interactions between the traps can be neglected, Smoluchowski[1] derived an expression for the trapping rate (rate constant) k for spherical traps. For arbitrary trap density, there will be a competition between traps and the trapping rate will depend upon the concentration of traps.[2] For spherical traps at high trap concentrations, a variety of techniques have been employed to obtain the trapping rate k, including effective-medium theories,[3] survival probability theory,[4,5] rigorous bounds,[6,7] and random-walk simulation techniques.[4,8-10]

Virtually no studies have been carried out to determine the trapping rate for statistically anisotropic distributions of traps, e.g., oriented ellipsoidal traps. Fredrickson and Shaqfeh[11] have recently examined the special case of distributions of slender, aligned rodlike traps at dilute to semidilute concentrations. More recently, Torquato and Lado[12] have obtained rigorous lower bounds on the trapping rate for random distributions of oriented spheroidal traps.

It is important to distinguish between *statistical* and *macroscopic* anisotropy.[13] Statistical anisotropy implies that the n-point correlation functions that statistically characterize the microstructure[7,13] do not remain invariant under rotation. Macroscopic anisotropy refers to anisotropy with respect to the properties of the heterogeneous system. The trapping rate is always macroscopically isotropic even when the microstructure is statistically anisotropic.

This paper reports Brownian-motion simulation results for the steady-state trapping rate k associated with diffusion in statistically anisotropic microgeometries consisting of oriented, spheroidal traps of arbitrary aspect ratio $\epsilon = b/a$ over a wide range of trap volume fractions $\phi_2 = 1 - \phi_1$ (where ϕ_1 is the porosity). The spheroidal traps are aligned parallel to the z axis with length $2b$ and maximum diameter $2a$. We consider obtaining k for several prolate cases ($\epsilon = 2$, 5, and 10) and oblate cases ($\epsilon = 0.1$, 0.2, and 0.5). These results are compared to data for spheres ($\epsilon = 1$) which we also compute. Both instances of overlapping (i.e., spatially uncorrelated) and nonoverlapping (i.e., spatially correlated) spheroidal traps shall be investigated. Thus we seek to probe the effects of both statistical anisotropy and spatial correlation of the traps on the trapping rate. Our simulation data will be compared to a rigorous lower bound on k for oriented spheroidal traps recently obtained by Torquato and Lado.[12]

The trapping rate is simply the inverse of the average survival time $\bar{t}$ for diffusing (Brownian) particles which is proportional to the total mean square displacement before trapping $\bar{r}^2$:[4,7]

$$k = \bar{t}^{-1} = 6D/\bar{r}^2. \tag{1}$$

This relationship is valid for statistically anisotropic media. Unlike recent random walk algorithms that simulate the detailed zig-zag motion of the diffusing particle with small,

 0021-9606/91/085592-07$03.00

finite step sizes,[4,8] the present investigation facilitates the calculation by using *first passage time* equations as was recently done by Torquato and Kim[10] for spherical traps. Torquato and Kim showed the use of a first passage time algorithm resulted in an execution time that is at least an order of magnitude faster than procedures which simulate the detailed zig-zag motion of the random walker.

Given our results for k, we shall also be able to obtain estimates for the fluid permeability tensor $\mathbf{K}$ associated with slow viscous flow through the same microgeometry by applying a recent theorem due to Torquato.[13] He rigorously proved that, for arbitrary statistically anisotropic porous media of porosity ϕ_1, the fluid permeability tensor $\mathbf{K}$ is related to the *trapping constant* γ by the following inequality:

$$\mathbf{K} \leqslant \gamma^{-1}\mathbf{I}, \tag{2}$$

where $\mathbf{I}$ is the identity tensor. Relation (2) states that the tensor $(\gamma^{-1}\mathbf{I} - \mathbf{K})$ is positive semidefinite. The trapping constant is trivially related to the trapping rate as

$$k = \gamma\phi_1 D. \tag{3}$$

Note $\mathbf{K}$ and γ^{-1} both have dimensions of (length).[2]

II. SIMULATION PROCEDURE

Obtaining the trapping rate k from our computer simulations is a two-step process. First, one must generate random realizations of the random medium, which in this study are distributions of oriented spheroidal traps. Second, employing a Brownian motion algorithm, we determine the total mean square displacement $\bar{r}^2$ and, thus, the trapping rate [cf. Eq. (1)].

Generating equilibrium distributions of spheres (with hard cores) using a Metropolis algorithm[14] is relatively straightforward. For nonspherical shapes, such as oriented *spheroids*, the generation of equilibrium configurations is considerably more involved. The generation of equilibrium realizations of oriented spheroids, however, is substantially simplified by exploiting the observation of Lebowitz and Perram[15] that a scale transformation to coordinates

$$\mathbf{R} \equiv (X,Y,Z) = [x,y,(a/b)z] \tag{4}$$

converts oriented spheroids of shape

$$(x^2 + y^2)/a^2 + z^2/b^2 = 1 \tag{5}$$

into spheres of radius a at the same volume fraction, thus reducing the thermodynamics and particle correlations of aligned hard (nonoverlapping) spheroids into an equivalent problem involving hard spheres. Here, X, Y, Z and x, y, z represent coordinates in the sphere and spheroid domains, respectively. This transformation actually also applies to *overlapping* (i.e., spatially uncorrelated) spheres.[12] Thus the Z coordinate in the sphere domain is mapped to

$$z = (b/a)Z \tag{6}$$

in the corresponding spheroid domain. Lado and Torquato[16] have recently computed the two-point matrix probability function S_2 for distributions of oriented hard spheroids using this scale transformation. Figures 1 and 2 depict two-dimensional distributions of oriented hard ellipses and oriented overlapping ellipses.

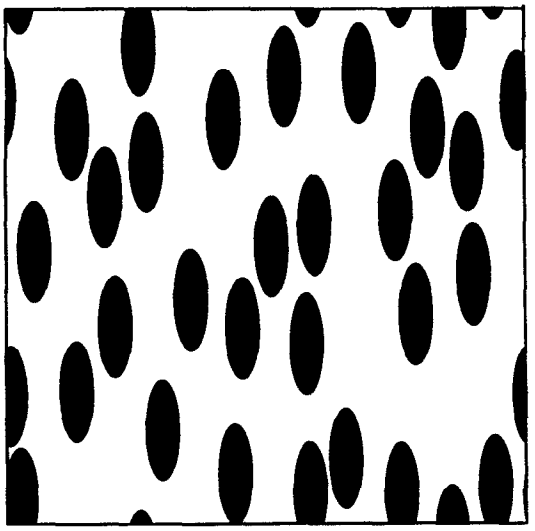

FIG. 1. A distribution of oriented impenetrable ellipses at an ellipse volume fraction $\phi_2 \approx 0.3$ and aspect ratio $\epsilon = b/a = 3$.

Therefore, we first generate realizations of spheres, then "stretch" the entire system according to (6) to obtain corresponding distributions of oriented spheroids of arbitrary aspect ratio ϵ. A standard Metropolis algorithm[14] is used to generate equilibrium configurations of overlapping and nonoverlapping spheres at sphere volume fraction ϕ_2. Then, N spheres of radius a are initially placed on lattice sites of a cubic array in a cubical cell of volume L^3. [Note that the reduced number density $\eta = (N/L^3)(4\pi/3)a^3$ is equal to the sphere volume fraction ϕ_2 only in the hard-sphere case. For overlapping spheres, $\phi_2 = 1 - \exp(-\eta)$.] The cell is surrounded by periodic images of itself. Each spherical particle is then randomly moved a small distance to a new position which is accepted only if no hard-core overlap exists. This process is repeated many times until equilibrium is achieved. To ensure equilibrium configurations have been generated, the simulation program measures the contact val-

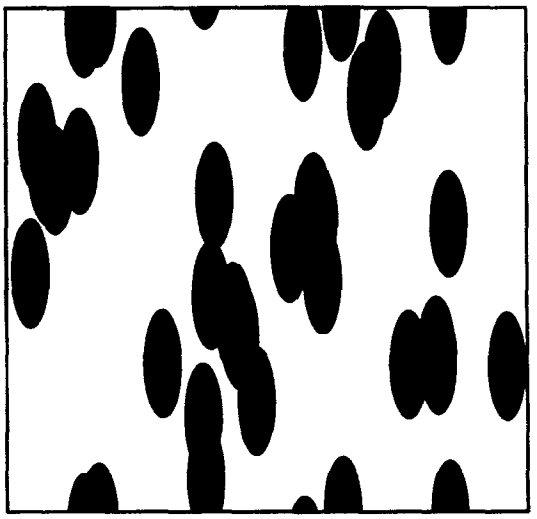

FIG. 2. A distribution of oriented overlapping ellipses at an ellipse volume fraction $\phi_2 \approx 0.3$ and aspect ratio $\epsilon = b/a = 3$.

ue of the pair or radial distribution function $g_2(2a)$, which is trivially related to the pressure of the system. In the case of hard spheres, the simulated value of g_2 at contact is then compared to the well-known and accurate Carnahan–Starling approximation.[17] The measured contact values of g_2 were found to be in excellent agreement with the latter.

Once a configuration of spheres has been generated, the system is "stretched" or "compressed" using the mapping (6), resulting in a configuration of randomly positioned oriented spheroids with volume fraction ϕ_2 or reduced number density η, and degree of penetrability identical to the original configuration of spheres in the cubical cell. It is in the spheroid domain that random walks are conducted.

The total mean-square displacement of Brownian particles before trapping $\bar{r}^2$ is computed using the first passage time algorithm of Torquato and Kim.[10] One first constructs the largest possible concentric sphere of radius r_i about the initial position of the Brownian particle that does not overlap any traps. Now since the average time t_i required for the Brownian particle to first strike the surface of the imaginary sphere of radius r_i is simply $r_i^2/6D$, then one need only randomly choose a point on this surface and record r_i. This process is repeated, each time keeping track of r_i until the walker is trapped; the total mean-square displacement per walker is Σr_i^2. The quantity $\bar{r}^2$ or the trapping rate is finally determined by averaging over many random walks and realizations. In practice, the Brownian particle is considered trapped when it comes within a very small distance δ of the trap surface. A further savings in computation time is made by checking distances only to traps nearest to the walker by employing the "Grid" method described by Lee *et al.*[8] Torquato and Kim[10] showed that for spherical traps this algorithm resulted in an execution time which is at least an order of magnitude faster than simulation methodologies that simulate the detailed zig-zag motion of the random walker with small finite step sizes.[4,8]

We employ this algorithm in the spheroidal case with the only difference being the part of the algorithm that checks for the minimum distance from a point to a trap surface, i.e., the radius of the first passage sphere. For spherical traps, the minimum distance is simply the distance between the sphere center and the point, minus the sphere radius. For spheroidal traps, however, determination of the minimum distance is somewhat more involved. Because the traps are symmetrical about their z axes, this problem reduces to determination of the minimum distance between a point and an ellipse, resulting in a quartic equation which can be solved analytically.[18]

In our simulations, each configuration contained 1000–1134 traps, $\delta/a = 0.0001$, and a total of 1000 walks per configuration were carried out. A total of 100 configurations were generated for each value of η and ϵ examined. Our calculations were carried out on a VAX station 3100 and a CRAY Y-MP.

III. RESULTS AND DISCUSSION

A. Trapping rate

Here we report computer simulation results for k of distributions of oriented spheroidal traps at values of the aspect ratio $\epsilon = 0.1$, 0.2, 0.5, 1, 2, 5, and 10 and trap volume fraction $\phi_2 = 0.1$, 0.3, and 0.5. Data for overlapping and nonoverlapping traps are given. In the case of hard spherical traps, $\phi_2 = 0.5$ corresponds to a value very close to the onset of the fluid–solid phase transition.[19]

Our data shall be compared to a rigorous lower bound on the trapping rate (or trapping constant) for oriented spheroidal traps obtained recently by Torquato and Lado.[12] These authors computed the general two-point "void" bound derived by Torquato and Rubinstein.[7] Specifically, Torquato and Lado found

$$k \geqslant k^{(2)} = (D\phi_1\phi_2^2/4a^2\langle x\rangle_o) f(\epsilon), \tag{7}$$

where

$$f\left(\frac{b}{a}\right) = \begin{cases} \dfrac{2\chi_b}{\ln[(1+\chi_b)/(1-\chi_b)]}, & b<a, \\ \chi_a/\tan^{-1}(\chi_a), & b>a \end{cases} \tag{8}$$

is a purely shape-dependent function with

$$\chi_a^2 = -\chi_b^2 = (b^2/a^2) - 1, \tag{9}$$

and the quantity

$$\langle x\rangle_o = \int_0^\infty x[S_2(x) - \phi_1^2]\,dx \tag{10}$$

is the first moment of the probability function $[S_2(x) - \phi_1^2]$ for the reference *spherical* system. Here, $S_2(r)$ is the probability of finding the end points of a line segment of length r in the trap-free region, ϕ_1^2 is its long-range value, and $x = r/2a$. Note that Torquato and Lado actually bounded the trapping constant that is simply related to k by relation (3).

For the values of volume fraction ϕ_2 and aspect ratio ϵ considered here, there are no other analytical expressions of k available. As a test case, however, we can conduct our simulations at very low volume fractions and compare to the exact infinitely dilute limit of k, denoted by k_s, for oriented spheroids. From the Appendix, we have

$$k_s = (3D\phi_2/a^2) f(\epsilon). \tag{11}$$

Note that (11) contains the same shape-dependent function $f(\epsilon)$ as the bound (7). In the infinitely dilute limit, Torquato and Rubinstein[7] showed that

$$\langle x\rangle_o \sim \phi_2/10. \tag{12}$$

Substitution of (12) into (7) gives

$$k \geqslant k^{(2)} = (5D\phi_2/2a^2) f(\epsilon) \quad (\phi_2 \ll 1). \tag{13}$$

Thus, in the infinitely dilute limit, the bound gives $5k_s/6$. Although bound (7) is not exact in this limit, it does reflect the proper shape dependence.

We carried out simulations of the trapping rate for a variety of aspect ratios in the range $0.1 \leqslant \epsilon \leqslant 10$ at trap volume fractions between 10^{-5} and 10^{-4} and found excellent agreement with the exact result (11).

Tables I and II summarize our data for the trapping rate for random distributions of oriented prolate and oblate spheroidal traps in tabular form. Table I gives results for the dimensionless trapping rate ka^2/D, whereas Table II gives results for the dimensionless trapping rate k/k_s. Note that

TABLE I. The dimensionless trapping rate ka^2/D for selected values of the trap volume fraction ϕ_2 and aspect ratio b/a in the cases of both overlapping and hard, oriented spheroidal trap distributions. Here, a is the semiaxis defined in the text and D is the diffusion coefficient.

	ka^2/D					
	Overlapping spheroids			Hard spheroids		
b/a	$\phi_2=0.1$	$\phi_2=0.3$	$\phi_2=0.5$	$\phi_2=0.1$	$\phi_2=0.3$	$\phi_2=0.5$
0.1	5.03	31.3	93.6	6.13	54.8	247.
0.2	2.19	12.0	34.0	2.69	21.6	94.9
0.5	0.874	4.43	11.5	1.08	8.10	34.3
1.0	0.513	2.50	6.52	0.633	4.68	19.4
2.0	0.345	1.73	4.52	0.430	3.20	13.5
5.0	0.257	1.35	3.59	0.313	2.42	10.4
10.0	0.231	1.24	3.38	0.279	2.23	9.59

the results for spheres ($b/a=1$) agree well with the results of Lee *et al.*[8] who computed k by simulating the detailed zigzag motion of the random walker.[20]

Figure 3 depicts the scaled trapping rate ka^2/D vs $\log(b/a)$ for both hard and overlapping spheroids with $\phi_2=0.1$. Included in the figure are the corresponding two-point bounds (7) computed by Torquato and Lado.[12] Figures 4 and 5 show corresponding results for $\phi_2=0.3$ and $\phi_2=0.5$, respectively. There are a number of noteworthy features. First, not surprisingly, ka^2/D increases with increasing trap volume fraction ϕ_2 for fixed aspect ratio for both *hard* and *overlapping* traps. Second, the data always lie above the rigorous lower bound, with the discrepancy between the two increasing with increasing ϕ_2, as expected. Third, for fixed ϕ_2 and b/a, the trapping rate for hard traps lies above the trapping rate for overlapping traps. This is expected since the specific surface (interfacial surface area per unit volume) of the former system is always greater than the specific surface of the latter for nonzero ϕ_2. Fourth, ka^2/D, for fixed ϕ_2, decreases with increasing aspect ratio; prolate and oblate results are always below and above the sphere results ($b/a=1$), respectively. Again, this is related

TABLE II. The dimensionless trapping rate k/k_∞ for selected values of the trap volume fraction ϕ_2 and aspect ratio b/a in the cases of both overlapping and hard, oriented spheroidal trap distributions. Here, k/k_∞ is the exact infinitely dilute-limit result (11).

	k/k_∞					
	Overlapping spheroids			Hard spheroids		
b/a	$\phi_2=0.1$	$\phi_2=0.3$	$\phi_2=0.5$	$\phi_2=0.1$	$\phi_2=0.3$	$\phi_2=0.5$
0.1	2.48	5.14	9.22	3.02	9.00	24.3
0.2	2.04	3.74	6.33	2.50	6.72	17.7
0.5	1.76	2.97	4.65	2.18	5.44	13.8
1.0	1.71	2.78	4.35	2.11	5.20	12.9
2.0	1.75	2.93	4.58	2.18	5.40	13.7
5.0	2.00	3.50	5.60	2.44	6.28	16.2
10.0	2.31	4.19	6.79	2.80	7.45	19.2

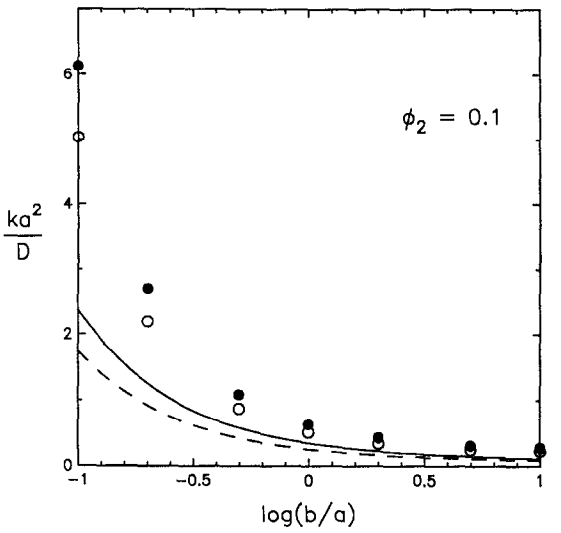

FIG. 3. The dimensionless trapping rate ka^2/D vs the log of the aspect ratio b/a for hard oriented spheroids and overlapping oriented spheroids at a spheroid volume fraction $\phi_2=0.1$. Filled and unfilled circles are the hard and overlapping simulation data, respectively. Solid and dashed lines, respectively, are the lower bounds (7) for hard and overlapping traps obtained by Torquato and Lado.[12]

to the fact that the surface area available for reaction decreases as b/a increases for fixed ϕ_2. Whereas k gradually changes as the aspect ratio b/a is varied for prolate spheroidal traps, k dramatically increases as the spheroids become disklike ($\epsilon \ll 1$). For the case of *hard oblate* traps, the data obtained for the range $0.1 \leqslant \epsilon \leqslant 1$ obeys the following power law:

$$ka^2/D \sim (b/a)^{-\alpha}, \tag{14}$$

where the exponent α (approximately unity) weakly depends on the trap volume fraction ($\alpha=0.99$ at $\phi_2=0.1$, $\alpha=1.07$ at $\phi_2=0.3$, and $\alpha=1.11$ at $\phi_2=0.5$).

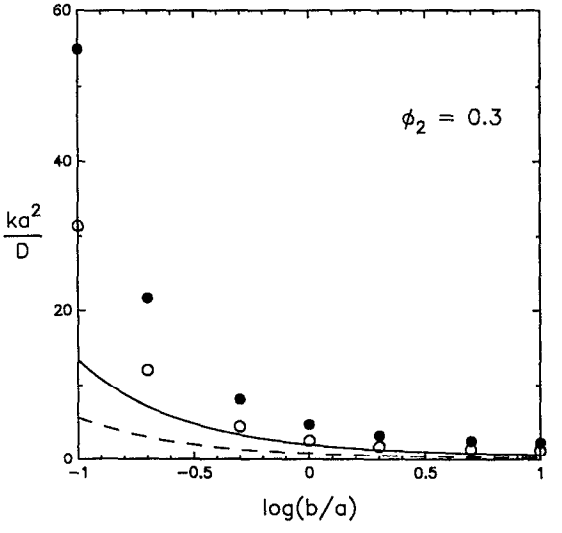

FIG. 4. As in Fig. 3 for $\phi_2=0.3$.

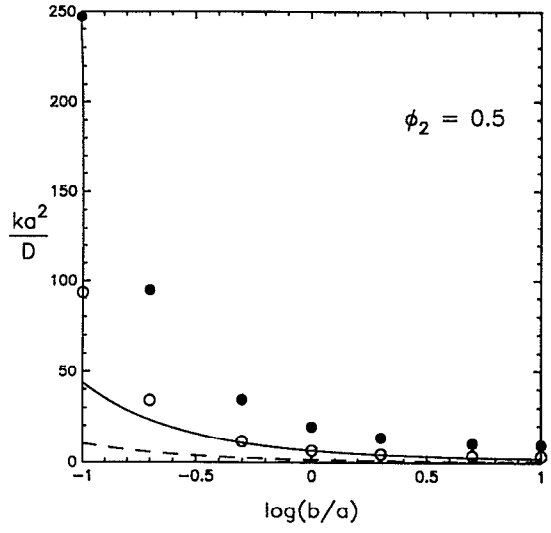

FIG. 5. As in Fig. 3 for $\phi_2 = 0.5$.

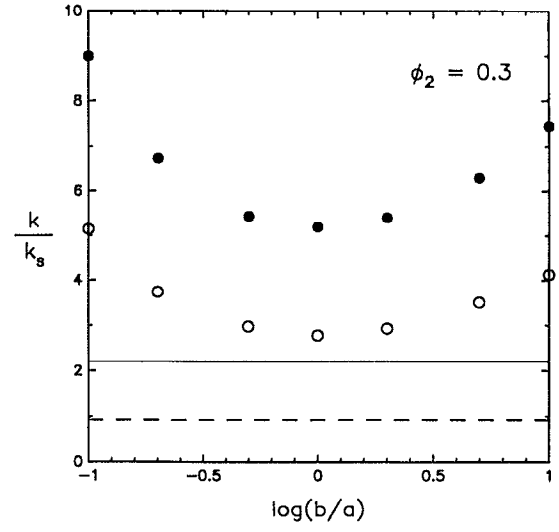

FIG. 7. As in Fig. 6 with $\phi_2 = 0.3$.

Figures 6–8 show the dimensionless trapping rate k/k_s vs $\log(b/a)$ for $\phi_2 = 0.1$, 0.3, and 0.5, respectively. Plotted in this fashion, for a certain range of ϕ_2 and b/a, we see that the symmetric relation

$$k(\epsilon)/k_s(\epsilon) = k(\epsilon^{-1})/k_s(\epsilon^{-1}) \tag{15}$$

is approximately obeyed. Expression (15) holds for small ϕ_2 ($\phi_2 < 0.1$) for a wide range of aspect ratios. It is also approximately satisfied for nearly spherical shapes ($0.5 < b/a < 2$) for all volume fractions reported. Interestingly, the bound (7) exactly obeys such a scaling, i.e., (7) and (11) combine to give

$$k^{(2)}(\epsilon)/k_s(\epsilon) = k^{(2)}(\epsilon^{-1})/k_s(\epsilon^{-1}). \tag{16}$$

The ratio $k^{(2)}(\epsilon)/k_s(\epsilon)$, however, for fixed ϕ_2, is independent of the aspect ratio, in contrast to the data.

In Figs. 9 and 10 we plot the dimensionless trapping rate k/k_s versus the trap volume fraction ϕ_2 for hard, prolate spheroids and hard, oblate spheroids, respectively. (Corresponding plots for the overlapping case are similar and hence are not shown.) Included in the figures are the associated lower bounds. Comparing Figs. 9 and 10 again confirms the validity of the symmetric relation (15) for the aforementioned range of parameters.

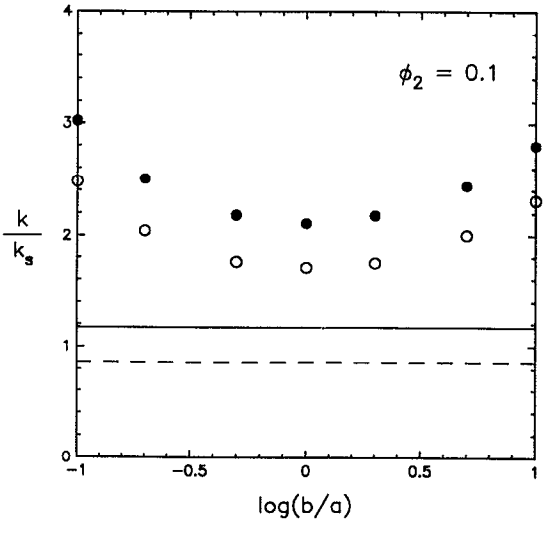

FIG. 6. The dimensionless trapping rate k/k_s versus the log of the aspect ratio b/a for hard oriented spheroids and overlapping oriented spheroids at a spheroid volume fraction $\phi_2 = 0.1$. Filled and unfilled circles are the hard and overlapping simulation data, respectively. Solid and dashed lines, respectively, are the lower bounds (7) for hard and overlapping traps obtained by Torquato and Lado.[12] Here, k_s is the exact infinitely dilute-limit result (11).

B. Fluid permeability tensor

Torquato[13] has shown that the fluid permeability tensor $\mathbf{K}$ for an anisotropic porous medium of arbitrary topology at porosity $\phi_1 (= 1 - \phi_2)$ is related to the trapping rate k of the same medium by the tensor relation (3). Thus the results of Table I for ka^2/D lead immediately to upper bounds on

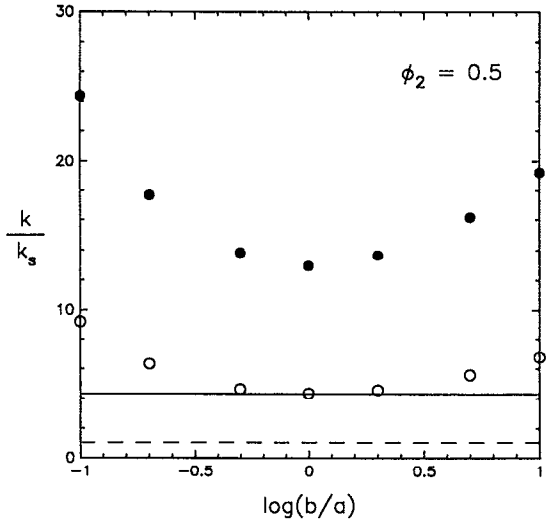

FIG. 8. As in Fig. 6 with $\phi_2 = 0.5$.

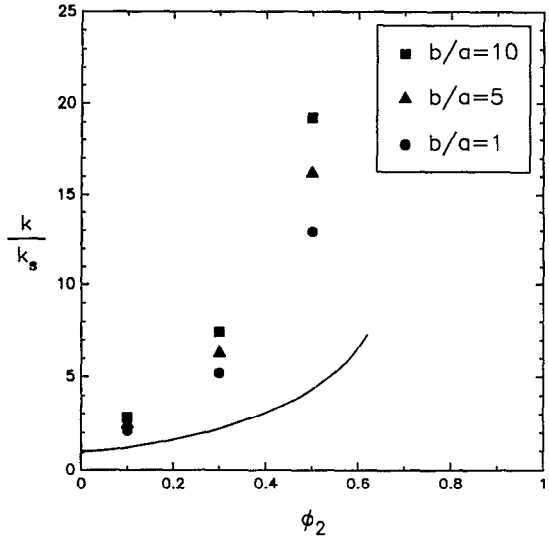

FIG. 9. The dimensionless trapping rate k/k_s versus spheroid volume fraction ϕ_2 for hard prolate traps at various aspect ratios. The solid line is the lower bound (7) for hard prolate spheroids[12] that is independent of aspect ratio.

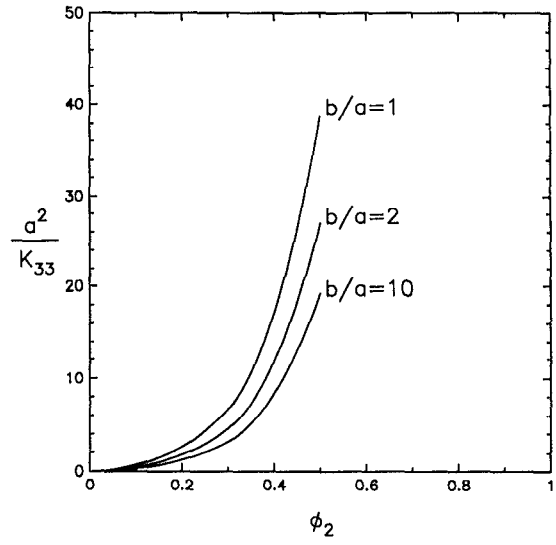

FIG. 11. Lower bounds on the dimensionless fluid resistance $a^2K_{33}^{-1}$ versus spheroid volume fraction ϕ_2 for hard prolate spheroids at various values of the aspect ratio b/a. The bounds are obtained by combination of relations (3), (17) and the results of Table I for the trapping rate. Solid lines are spline fits of the data so obtained.

the eigenvalues of $\mathbf{K}$, which we denote by K_{ii}, or lower bounds on K_{ii}^{-1}, where $\mathbf{K}^{-1}$ is the fluid *resistance* tensor. If we let the x_3 direction be parallel to the axis of symmetry, then from (3) we have

$$\begin{bmatrix} K_{11}^{-1} & 0 & 0 \\ 0 & K_{11}^{-1} & 0 \\ 0 & 0 & K_{33}^{-1} \end{bmatrix} \geqslant \begin{bmatrix} \gamma & 0 & 0 \\ 0 & \gamma & 0 \\ 0 & 0 & \gamma \end{bmatrix}, \tag{17}$$

where γ (the trapping constant) is related to k (the trapping rate) by relation (3). Here we have used the fact that $K_{11} = K_{22}$. Note that the trapping constant tensor is isotropic as discussed in the Introduction. Now for prolate spheroids, $K_{11}^{-1} > K_{33}^{-1}$, and thus the bound on K_{33}^{-1} will be sharper than the bound on K_{11}^{-1}. On the other hand, for oblate spheroids, $K_{11}^{-1} < K_{33}^{-1}$ and so the bound on K_{33}^{-1} will be weaker than the bound on K_{11}^{-1}. The results of Table I and Eqs. (3) and (17) show that the resistance K_{ii}^{-1} in the x_i direction increases with increasing concentration of spheroids ϕ_2, as expected. In Fig. 11, we plot the dimensionless resistance $a^2K_{33}^{-1}$ versus volume fraction for the case of hard prolate spheroids at various aspect ratios.

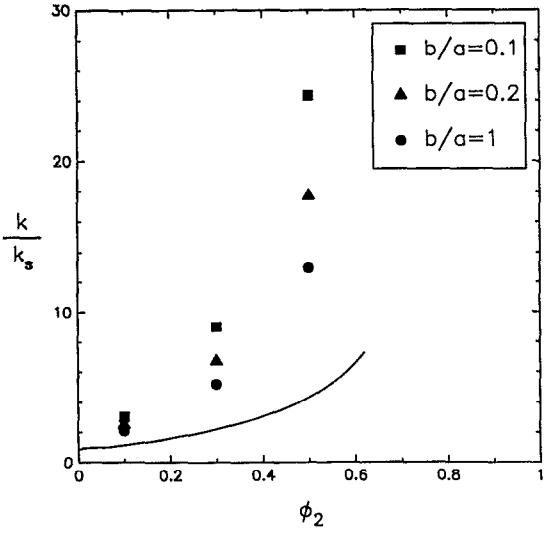

FIG. 10. As in Fig. 9 for hard, oriented oblate spheroids.

ACKNOWLEDGMENTS

The authors gratefully acknowledge the support of the Office of Basic Energy Sciences, U.S. Department of Energy under Grant No. DE-FG05-86ER13482. Some computer resources (CRAY Y-MP) were supplied by the North Carolina Supercomputer Center funded by the State of North Carolina.

APPENDIX: BOUNDARY-VALUE PROBLEM FOR AN ISOLATED SPHEROIDAL TRAP AND THE DILUTE-LIMIT TRAPPING RATE

Here we present solution details of the boundary value problem for an isolated spheroidal trap. From this solution we obtain the infinitely dilute limit trapping rate k_s. In general, the equation describing the concentration c of reactant species about a single trap of arbitrary shape is given by

$$\nabla^2 c = 0 \tag{A1}$$

in the trap-free region with boundary conditions

$$c(\mathcal{S}) = 0, \tag{A2}$$

$$c(r \to \infty) = \bar{c}, \tag{A3}$$

where $\bar{c}$ is the average concentration over the trap-free region, and $\mathcal{S}$ denotes the trap surface. In prolate spheroidal coordinates,[21]

$$\nabla^2 c = \frac{1}{\alpha^2(\sinh^2\eta + \sin^2\theta)} \times\left[\frac{\partial^2 c}{\partial\eta^2} + \coth\eta\,\frac{\partial c}{\partial\eta} + \frac{\partial^2 c}{\partial\theta^2} + \cot\theta\,\frac{\partial c}{\partial\theta}\right] + \frac{1}{\alpha^2\sinh^2\eta\sin^2\theta}\,\frac{\partial^2 c}{\partial\psi^2}, \tag{A4}$$

where $\alpha = \sqrt{b^2 - a^2}$, a and b being the semiminor and semimajor axes of the spheroid, respectively. The trap surface defined by $\eta = \eta_0$ is related to a and b through

$$a = \alpha\sinh\eta_0, \tag{A5}$$

$$b = \alpha\cosh\eta_0. \tag{A6}$$

The boundary conditions (A2) and (A3) become, respectively,

$$c(\eta = \eta_0) = 0, \tag{A7}$$

$$c(\eta\to\infty) = \bar{c}. \tag{A8}$$

Clearly $c = c(\eta)$ only, and so (A1) reduces to

$$\frac{d^2 c}{d\eta^2} + \coth\eta\,\frac{dc}{d\eta} = 0, \tag{A9}$$

which, with boundary conditions (A7) and (A8), yields

$$c(\eta) = \bar{c}\left[1 - \frac{\ln\coth(\eta/2)}{\ln\coth(\eta_0/2)}\right], \tag{A10}$$

which is the species concentration about a single prolate spheroidal trap. The total reactant flux J_t into a single isolated trap is given by

$$J_t = -D\int_{\mathscr{S}} \nabla c(\eta = \eta_0)\cdot\hat{n}\,d\mathscr{S}, \tag{A11}$$

where $\hat{n}$ is the unit vector normal to the trap surface. Carrying out indicated operations yields

$$J_t = \frac{4D\pi\bar{c}\alpha}{\ln\coth(\eta_0/2)}. \tag{A12}$$

For steady-state conditions in a field of N widely spaced traps (i.e., negligible competition between traps), the reactant flux into all traps (the total trapping rate) is exactly equal to the rate of production of the reactant over the entire volume V, or

$$NJ_t = Vk_s\bar{c}. \tag{A13}$$

Since $\cosh\eta_0 = b/\alpha$, $\sinh\eta_0 = a/\alpha$, and $\rho = N/V$, substituting (A12) into (A13) yields (after simple algebra)

$$k_s = 4D\pi\rho a\left[\sqrt{\epsilon^2 - 1}/\ln(\epsilon + \sqrt{\epsilon^2 - 1})\right]. \tag{A14}$$

In general, as the volume fraction of traps approaches zero, $4\pi\rho a$ approaches $3\phi_2/(a^2\epsilon)$ (note that this relation is always true for impenetrable traps). Then rearranging terms, (A14) yields the infinitely dilute limit

$$k_s = \frac{3D\phi_2}{a^2}\,\frac{2\chi_a}{\ln[(1+\chi_a)/(1-\chi_a)]}. \tag{A15}$$

For oblate spheroidal traps, (A1) takes the form[21]

$$\frac{d^2 c}{d\eta^2} + \tanh\eta\,\frac{dc}{d\eta} = 0, \tag{A16}$$

which with conditions (A7) and (A8) results in

$$c(\eta) = \bar{c}\left[1 - \frac{\cot^{-1}\sinh\eta}{\cot^{-1}\sinh\eta_0}\right]. \tag{A17}$$

Following the same procedure as above, we find

$$k_s = 4D\pi\rho\left[\alpha/\cot^{-1}(\sinh\eta_0)\right]. \tag{A18}$$

With some straightforward rearrangement, for $\phi_2\to 0$, the above yields

$$k_s = (3D\phi_2/a^2)(\chi_b/\tan^{-1}\chi_b). \tag{A19}$$

[1] M. V. Smoluchowski, Phys. Z. **17**, 557 (1916).
[2] B. U. Felderhof and J. M. Deutch, J. Chem. Phys. **64**, 4551 (1976).
[3] M. Muthukumar, J. Chem. Phys. **76**, 2667 (1982); R. I. Cukier and K. F. Freed, J. Chem. Phys. **78**, 2573 (1983); C. W. J. Beenakker and J. Ross, J. Chem. Phys. **84**, 3857 (1986); M. Fixman, J. Chem. Phys. **81**, 3666 (1984).
[4] P. M. Richards, Phys. Rev. Lett. **56**, 1838 (1986); J. Chem. Phys. **85**, 3520 (1986); Phys. Rev. B **35**, 248 (1987).
[5] A. Szabo, R. Zwanzig, and N. Agmon, Phys. Rev. Lett. **61**, 2496 (1988).
[6] M. Doi, J. Phys. Soc. Japan **40**, 567 (1976); D. R. S. Talbot and J. R. Willis, Proc. R. Soc. Lond. Ser. A **370**, 351 (1980); J. Rubinstein and S. Torquato, J. Chem. Phys. **88**, 6372 (1988).
[7] S. Torquato and J. Rubinstein, J. Chem. Phys. **90**, 1644 (1989).
[8] S. B. Lee, I. C. Kim, C. A. Miller, and S. Torquato, Phys. Rev. B **39**, 11833 (1989).
[9] L. H. Zheng and Y. C. Chiew, J. Chem. Phys. **90**, 322 (1989).
[10] S. Torquato and I. C. Kim, Appl. Phys. Lett. **56**, 1847 (1989).
[11] G. H. Fredrickson and E. S. G. Shaqfeh, Phys. Fluids A **1**, 3 (1989).
[12] S. Torquato and F. Lado, J. Chem. Phys. **94**, 4453 (1991).
[13] S. Torquato, Phys. Rev. Lett. **64**, 2644 (1990).
[14] N. Metropolis, A. W. Rosenthal, M. N. Rosenbluth, A. N. Teller, and E. Teller, J. Chem. Phys. **21**, 1087 (1953).
[15] J. L. Lebowitz and J. W. Perram, Mol. Phys. **50**, 1207 (1983).
[16] F. Lado and S. Torquato, J. Chem. Phys. **93**, 5912 (1990).
[17] N. F. Carnahan and K. E. Starling, J. Chem. Phys. **51**, 635 (1969).
[18] *CRC Standard Mathematical Tables* (CRC, Boca Raton, FL, 1981).
[19] J. P. Hansen and I. R. McDonald, *Simple Theory of Liquids* (Academic, New York, 1986).
[20] Trapping rate data for spherical traps reported in Ref. 8, although in good agreement with corresponding results of the present study, are not as accurate as the data here at large ϕ_2.
[21] P. E. Moon and D. E. Spencer, *Field Theory for Engineers* (Van Nostrand, Princeton, NJ, 1961); see also P. Moon and D. E. Spencer, *Field Theory Handbook* (Springer-Verlag, Berlin, 1988).